UNIVERSITY *of* York

This is a repository copy of *A novel NiO-based p-i-n ultraviolet photodiode*.

White Rose Research Online URL for this paper:
https://eprints.whiterose.ac.uk/193959/

Version: Accepted Version

**Article:**

White Rose
university consortium
Universities of Leeds, Sheffield & York

# A Novel NiO-based p-i-n Ultraviolet Photodiode

Fahrettin Sarcan[1*], Ümit Doğan[1], Ahmad Althumali[2,3], Hari B. Vasili[2], Leonardo Lari[2,4],

Adam Kerrigan[4], Furkan Kuruoğlu[1], Vlado K. Lazarov[2,4] and Ayşe Erol[1]

*corresponding author: fahrettin.sarcan@istanbul.edu.tr

[1] Department of Physics, Faculty of Science, Istanbul University, Vezneciler, 34134, Istanbul, Turkey

[2] School of Physics, Engineering and Technology,  University of York, Heslington, York, YO10 5DD, UK

[3] Department of Physics, Faculty of Science, Taif University, P.O. Box 11099, Taif 21944, Saudi Arabia

[4] The York-JEOL Nanocentre, University of York, Heslington, York, YO10 5BR, UK

Keywords: NiO; n-type NiO; p-type NiO; ultraviolet photodiode; p-i-n junction; wide bandgap; Franz–Keldysh.

**Abstract:**

In this study, the electrical and optical properties of a novel NiO-based homojunction p-i-n photodiode are reported. The p-i-n diode structure consists of Mg-doped, intrinsic and Cu-doped NiO from the top to the bottom layers, respectively. The photodiode structure was grown on a 0.7% Nb-doped $SrTiO_3$ (001) substrate using molecular beam epitaxy. The homojunction p-type NiO:Mg/i-NiO/n-type NiO:Cu exhibits diode characteristics. The ideality factor and barrier height of the diode are found to be 1.26 and 0.66 eV, respectively. The photoconductive properties of the photodiode were investigated by operating the diode under reverse bias, and spectral excitation of a Xe lamp. The responsivity of the photodiode is determined to be 295 mA/W at 3.9 eV. A constant photoresponse of the p-i-n photodiode between 3.75 eV and 6 eV with a responsivity of 250 mA/W is observed.

**Introduction:**

NiO is a promising wide bandgap ($E_g$~3.7 eV) material for ultraviolet optoelectronic applications. So far, NiO has been used as a hole transport layer in perovskite based solar cell applications due to its p-type characteristic in nature [1-3] and in ultraviolet metal-semiconductor-metal photodetectors applications due to its wide bandgap and larger resistivity [4-7]. Besides, it has been utilised as a p-type layer of NiO-based p-n and p-i-n junctions photodetectors.  [4–7]. In UV optoelectronic applications,  GaN, AlGaN and AlGaP have been usually preferred and these materials require good crystalline quality, which can obtained by epitaxial techniques. On the other hand, it has been shown that NiO is not only grown by

epitaxial techniques such as molecular beam epitaxy (MBE) [8–10], but also magnetron sputtering [11], pulsed laser deposition (PLD)[12], physical vapour deposition (PVD)[13], chemical vapour deposition (CVD)[14], Sol-Gel method[15].

Modern optoelectronic and electronic devices are based on p-n and p-i-n junctions. Although there are several NiO-based p-n and p-i-n junctions photodetector studies in the literature, these are not in homojunction structure due to the challenge of making n-type doped NiO. Studies in the literature have been mainly focused on the heterostructures that comprised of a p-type NiO and n-type of other semiconductors such as ZnO[16–20] $TiO_2$ [21,22] and $Ga_2O_3$[23,24] for UV applications, and n-type Si[25,26] for UV-visible applications. While these kinds of NiO-based, highly sensitive, heterojunctions are utilized as a photodetector, to create NiO-based emitters the fabrication of homojunction p-n and p-i-n diodes are critical.

It is well known in the literature that Mg doping enhances the hole transport properties of NiO when grown via MBE [4,27]. Cu doping, however, is an open topic with current studies mainly looking at magnetron sputtered films, with both p-type and n-type carriers being reported [28,29]. The p-type resistivity reported for NiO comes from nonstoichiometry in the samples, with Ni vacancies creating $Ni^{3+}$ sites which facilitate hole creation and transport. Furthermore, it has been shown that p-type resistivity can only be present in Cu-doped NiO if there are Ni vacancies present [30]. In this work, MBE is employed to produce films of high stoichiometry and crystallinity, hence the so-called 'intrinsic' p-type nature of NiO should not be present. This allows for the fabrication of a novel homojunction incorporating NiO:Mg | NiO | NiO:Cu into a p-i-n diode for which we provide growth and characterization studies.

**Experimental details:**
The p-i-n homojunction was epitaxially grown on (001)-oriented 0.7% Nb-doped $SrTiO_3$ (STO) substrate by MBE. Before the growth, the substrate was sequentially cleaned with acetone, isopropanol and DI water for 15 minutes each, in an ultrasonic bath. The substrate was then annealed at 950℃ for an hour in a furnace at atmospheric pressure, which was followed by MBE *in-situ* annealing at 600℃ in an oxygen environment with a partial pressure of $5\times10^{-6}$ mbar for 30 minutes. All layers were grown for an hour each at a substrate temperature of 300℃ and an oxygen partial pressure of $5\times10^{-6}$ mbar. First, $Ni_{0.5}Cu_{0.5}O$ layer was deposited

with Ni and Cu effusion cell temperatures of 1300℃ and 925℃, respectively. Then $Ni_{0.75}Cu_{0.25}O$ layer was grown with Ni and Cu effusion cell temperatures of 1300℃ and 825℃, respectively. The NiO layer was fabricated with a Ni effusion cell temperature of 1325℃. Finally, the $Ni_{0.75}Mg_{0.25}O$ layer was grown with Ni and Mg effusion cell temperatures of 1325℃ and 275℃, respectively. X-ray diffraction (XRD) $2\theta - \omega$ scan was used to determine the crystal structure and the epitaxial match between the substrate and the grown films. Cross-sectional scanning transmission electron microscopy (STEM) specimen was prepared by using an FEI Nova 200 NanoLab focused ion beam (FIB), using a standard lift-out method. A JEOL ARM200CF transmission electron microscope (TEM) was utilized for high-angle annular dark field (HAADF-STEM) imaging and energy-dispersive X-ray spectroscopy (EDX).

The diode fabrication steps were carried out using conventional photolithography techniques. A ring window with a diameter of 400 μm was patterned on the top of the diode. Layers of Au and Ni, with thicknesses of 60 nm and 10 nm respectively, were deposited by thermal evaporation for the top contact, while silver paste was used for the bottom contact. The current-voltage (I-V) characteristics of the diode were studied by an Agilent B2902A source/meter unit at room temperature. The capacitance-voltage (C-V) measurements were carried out by an HP4192A impedance spectrometer. The voltage was swept from positive to negative and negative to positive in the range of +2.5 V and -2.5 V. The C-V measurement was also studied at the various AC frequencies (100 kHz, 300 kHz and 1 MHz) in the given voltage ranges to enlighten the charge dynamics of the p-i-n diode. The spectral photocurrent measurements were carried out using a 0.5 m Jarrell-Ash monochromator with 0.5 nm spectral resolution. Xe lamp was used as an excitation source and the irradiated active area of the device was 0.125 $mm^2$. A mechanical chopper modulated the incident light at a frequency of 133 Hz, and a lock-in amplifier (SRS-830) was used to determine the photocurrent of the p-i-n photodiode. The measured photocurrent was converted to absolute responsivity by using a calibrated Si photodetector to measure the spectral intensity of the light source.

## Results and discussions
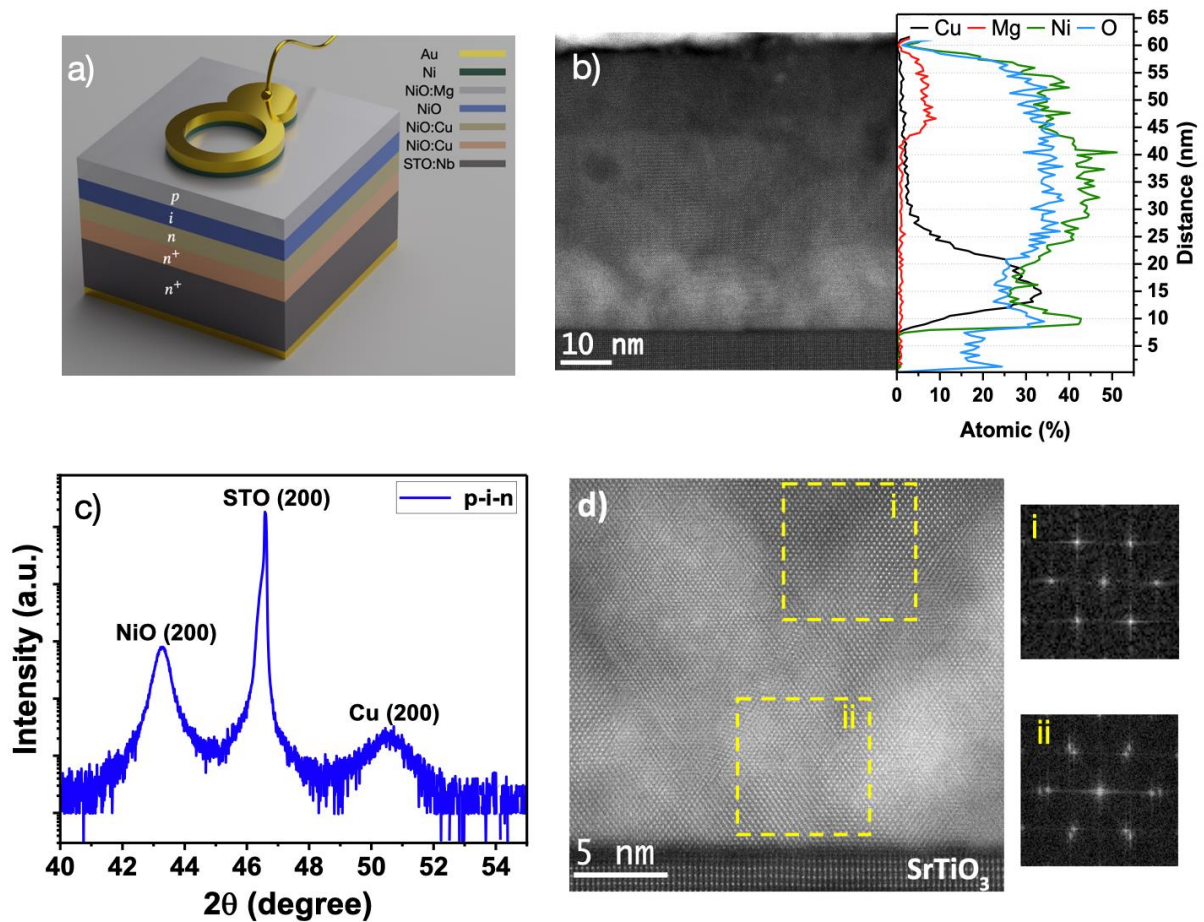


**Figure 1. a)** A schematics of photodiode structure, **b)** Cross-sectional HAADF-STEM image of the p-i-n diode on STO (001) substrate and corresponding EDX chemical averaged line profiles along its layers, **c)** XRD pattern of the p-i-n diode, and d) HAADF-STEM image of interface region corresponding to $Ni_{0.5}Cu_{0.5}O$ layer, with digital diffractograms from a region where Cu is fully soluble in the host NiO lattice (i), and a region where metallic Cu grains coexist with Cu doped/alloyed NiO (ii).

Figure 1a shows a schematic of the device alongside a cross-sectional HAADF-STEM image of the novel p-i-n diode (Figure 1b) grown epitaxially on the STO (001) by MBE, and the corresponding EDX averaged line profiles of its layers. The overall thickness of the diode is 55 nm as shown by the HAADF, which additionally confirms a smooth homojunction surface. The EDX chemical averaged line profiles present the atomic percentage distribution of Ni, O, Cu, and Mg elements across the device. Figure 1c shows $2\theta - \omega$ scan XRD for the homojunction p-i-n diode grown on the STO (001) substrate. The XRD result shows (002) reflections for the rock-salt crystal structure NiO, the perovskite crystal structure STO and the presence of Cu (002) peak indicating metallic Cu *fcc* grains. A closer look at the interface layer by HAADF

high-resolution image shows that within the nominal $Ni_{0.5}Cu_{0.5}O$ layer besides the NiO host lattice Cu metal grains are present, and they are fully commensurate with the lattice structure of the NiO film, as indicated by the digital diffractograms (i) and (ii) taken from selected regions shown in Figure 1d. This is also evident in the EDX spectra where the level of oxygen and Ni atomic percentage falls in regions (layer) with high Cu concentration, indicating that Cu is replacing Ni and also precipitating in Cu grains, in difference to Mg doped region of NiO where the Mg is purely substitutional of Ni.
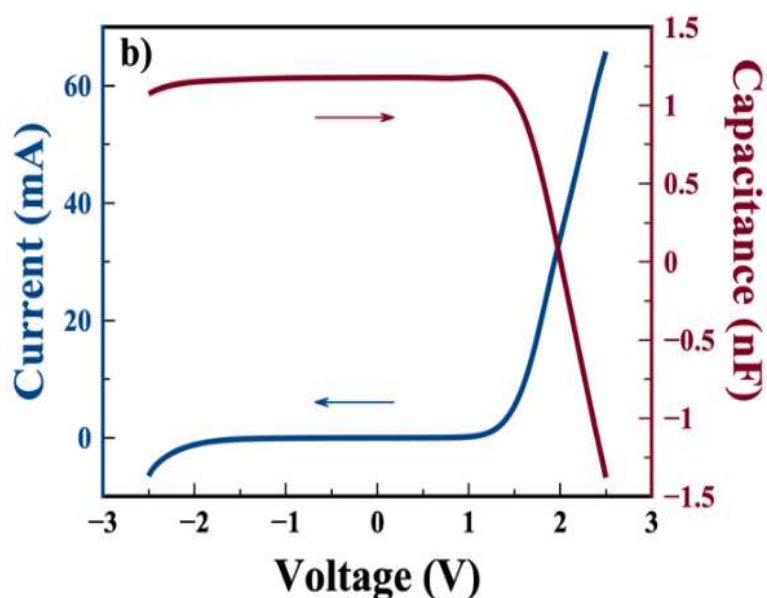


**Figure 2.** Current-voltage characteristic and capacitance-voltage characteristic of homojunction p-NiO:Mg/i-NiO/n-NiO:Cu diode under dark condition.

Figure 2 shows the current-voltage curves of the diode at room temperature, which demonstrates that the junction possesses diode characteristics with 38 mA and 1 mA current under 2 V forward and -2 V reverse bias, respectively. The dark current is 60 $\mu A$ at 1 V, increasing to 1 mA at 2 V. The main reason for the high current could be the carrier injection from the defect states and the diffusion of the current from around the ring contact because of the non-etched device structure. The capacitance *versus* voltage characteristic at 1MHz AC frequency is presented in Figure 2. In the low applied voltage range (<1.25 V), it shows a p-i-n diode behaviour as deduced from the general diffusion capacitance theory and Shockley's semiconductor theory; the capacitance decreases with reverse bias, while increases with the forward bias. As the forward bias is further increased, the capacitance decreases rapidly to

negative values, a phenomenon previously reported in the literature where it is attributed to the emitted carriers from the defect states[31-37].

For a detailed understanding of diode electrical properties, the diode parameters such as ideality factor, barrier height, series resistance, etc. have been determined by analyzing the current-voltage measurements in dark ambient conditions. According to the conventional thermionic emission (TE) theory [38,39], the forward current through a diode at a forward bias is given by the following equation,

$$I = I_0 \left[ exp \left( \frac{q(V - IR_S)}{nk_BT} \right) - 1 \right]$$

(1)

where $T$ is the temperature in Kelvin, $k_B$ is the Boltzmann's constant, $q$ is the electronic charge, $V$ is the applied bias voltage, which is greater than or equal to $3k_BT/q$ at small applied voltages, $n$ is the ideality factor and $I_0$ is the reverse saturation current obtained from the intercept point of the line at zero applied voltage and the following equation,

$$I_0 = AA^*T^2 exp \left( -\frac{q\Phi_b}{k_BT} \right)$$

(2)

where $A^*$ is the effective Richardson constant, which is taken from literature as 96 Acm$^{-2}$K$^{-2}$ for NiO[38], $A$ is the effective contact area and $\Phi_b$ is the zero bias potential barrier height. The ideality factor and barrier height ($\Phi_b$) can be determined by the following expressions,

$$n_{ideality} = \frac{q}{k_BT} \left( \frac{\partial lnln\, I}{\partial\, V} \right)^{-1}$$

(3)

and

$$\Phi_b = (k_BT)\, ln\, ln \left( \frac{AA^*T^2}{I_0} \right)$$

(4)

respectively.

The barrier height can also be determined from Norde's method [40,41]. According to this method, barrier height, as well as series resistance, can be determined from analysis of the following expression,

$$F(V) = \frac{V}{\gamma} - \frac{q}{k_B T} \ln \ln \left( \frac{I}{AA^*T^2} \right) \tag{5}$$

where $\gamma$ is the integer (dimensionless) greater than $n$. F(V) - voltage (V) plot is given in Figure 3a. The barrier height and series resistance of the diode can be determined by substituting $F(V_{min})$ and current value ($I_{min}$) corresponding to $V_{min}$ in Figure 3a into the following equations

$$\Phi_b = F(V_{min}) + \frac{V_{min}}{\gamma} - \frac{k_B T}{q} \tag{6}$$

$$R_s = \frac{k_B T (\gamma - n)}{q I_{min}} \tag{7}$$

Furthermore, the ideality factor, barrier height and series resistance of the diode can also be determined by dV/d(ln I) – current curve using the Cheung method as [38,42],

$$\frac{dV}{d(\ln \ln I)} = I R_s + n \left( \frac{kT}{q} \right) \tag{9}$$

$$(I) = V - n \left( \frac{kT}{q} \right) \ln \ln \left( \frac{I}{AA^*T^2} \right) \tag{10}$$

respectively. The experimental dV/dln(I) *versus I* and the *H(I) versus I* are demonstrated in Figure 3b. The ideality factor and barrier height are calculated from the intercept of dV/dln(I) *versus I* plot and *H(I) versus I* plot, respectively. The value of $R_s$ can also be obtained from the slopes of the dV/dln(I) *versus I* plot and *H(I) versus I* plot.
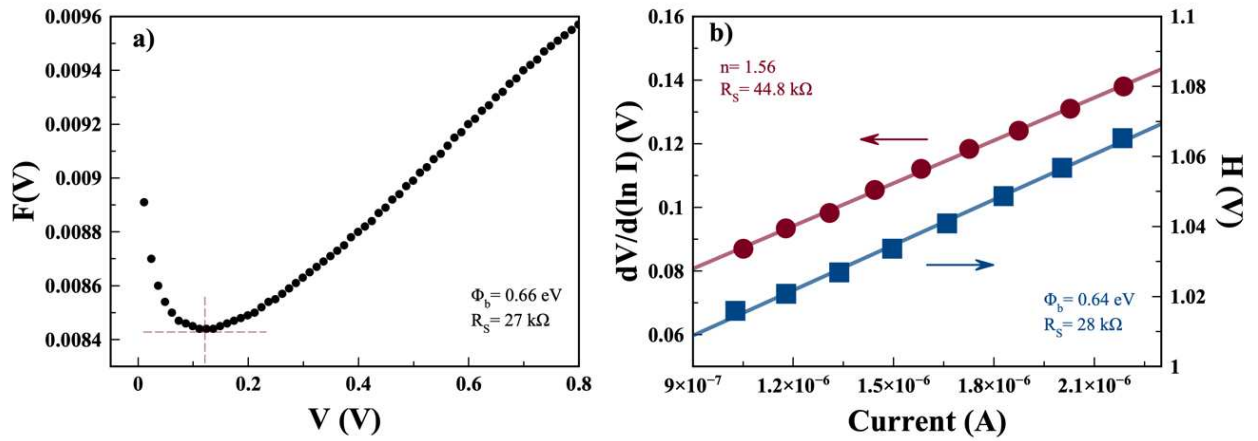
**Figure 3. a)** F(V) as a function of V, **b)** dv/d(ln(I)) and H (V) as a function of current.

All obtained diode parameters are listed in Table 1. These results show that the values of diode parameters obtained using different models are in good agreement with each other. The barrier height obtained from the different methods is $0.66 \pm 0.03$ eV. As the barrier height is simply the difference between the affinities of the p- and n-type layers this proves that the given structure has a diode characteristic.

**Table 1**. Electrical parameters of p-type NiO / i-NiO / n-type NiO homojunction p–i–n diode determined from three different methods

| I-V Characteristic | | Norde method | | dV/d(ln I) | | Cheung Method | |
|---|---|---|---|---|---|---|---|
| $n$ | $\Phi_b$(eV) | $\Phi_b$(eV) | $R_s$ ($\Omega$) | $n$ | $R_s(\Omega)$ | $\Phi_b$(eV) | $R_s(\Omega)$ |
| 1.26 | 0.69 | 0.66 | $2.7x10^4$ | 1.55 | $4.4x10^4$ | 0.64 | $2.8x10^4$ |

The obtained ideality factor of the diode is 1.26 and 1.55 from Eq. 3 and the intercept of the dV/dln(I) - I plot, respectively. An ideality factor of between 1 and 2 is an indication that both diffusion and recombination-based current mechanisms contribute to the forward bias current. The slight differences in the ideality factors likely come from the difference in the methods used. While the value corresponding to the lowest applied voltage is used in Eq.3, the intercept of the dV/dln(I) – I covers higher applied voltage values. The latter method, using the high voltage higher ideality, is attributed to radiative recombination-based current mechanisms which are compatible with the negative capacitance effect given in Figure 2 [36].
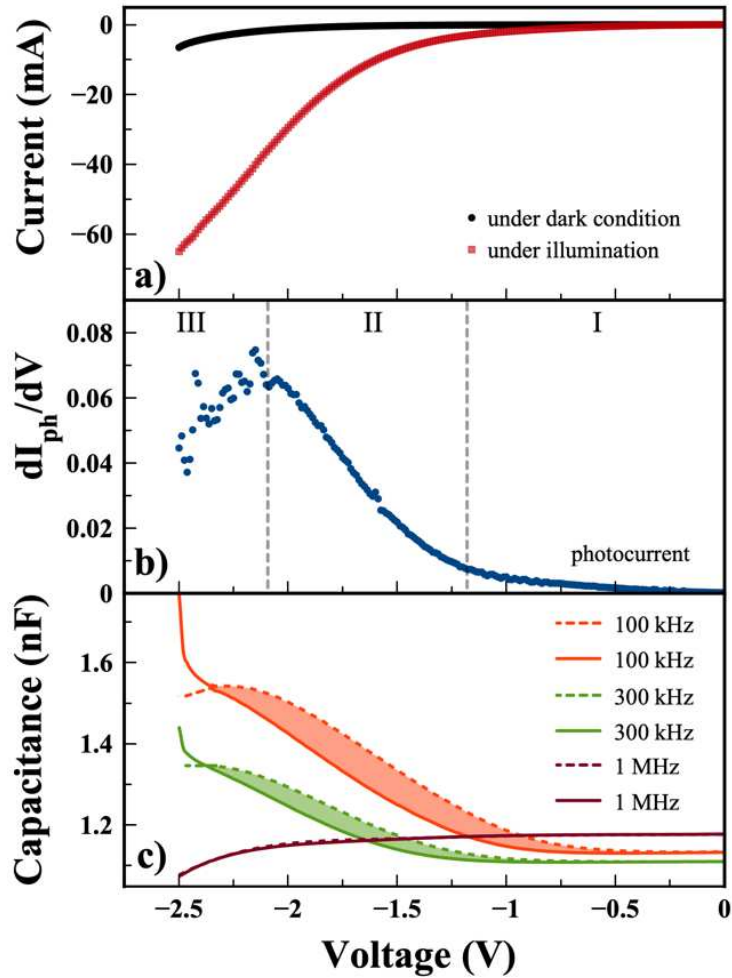
**Figure 4. a)** The current-voltage characteristic in dark and illumination conditions (Xe lamp, 150 W), **b)** derivation of photo current-voltage characteristic and **c)** capacitance-voltage of the diode. The dashed lines represent a voltage sweep from -2.5 V to +2.5V while the solid lines show the sweep from the other direction.

Furthermore, we have investigated the photoconductive properties of the photodiode. Figure 4a shows the current-voltage (reverse) characteristic under dark and illumination conditions (Xe lamp, 150 W). The total current ($I_{dark} + I_{ph}$) generated under the Xe lamp follows the dark current trend as a function of voltage, in the low current region up to ~1.25 V. After this, the total current deviates from the dark current, resulting in a drastic increment in photocurrent. The dependence of current on the bias voltage becomes clearer when we plot the deviation of $I_{ph}$ with respect to the applied voltage as depicted in Figure 4b [43,44]. While at low voltage range (Region I) $I_{ph}$ exhibits an almost ohmic behaviour as expected for p-i-n photodiodes, above -1.25 V biases $I_{ph}$ increases exponentially up to -2.1 V (Region II) then saturates. The high photocurrent, in Region II, originates from the carriers released from the trap such as deep-

level states and interface states due to photon assistance and expanding the depletion layer over the interfaces between the layers [45]. Above -2 V, Region III, due to the 20 nm thickness active layer, the electric field reached above $1 \times 10^6 V/cm$, which can cause strong bending and the barrier width becomes narrow, and the tunnelling current becomes dominant. The reduction in the active area and tunnelled carriers cause a decrease in the photogeneration rate, which results in a low photocurrent.

The capacitance-voltage (C-V) was plotted under the reverse bias for the different AC frequencies in Figure 4c and supports the $I_{ph}$ trend. The C-V shows a conventional diode characteristic for 1 MHz of AC frequencies, and it slightly decreases over the whole applied voltage range [36,46]. For the low AC frequencies, an increment was observed in the capacitance under the high reverse bias, Region II. In addition, a hysteresis between the bi-directional C-V curves was observed, which becomes stronger in the lower AC frequencies. These C-V trends and the bi-directional hysteresis under reverse bias can also be attributed to the existence of the deep-level states and interface states [47–49]. In light of these results, it can be concluded that -1.25 V < $V_b$ < -2.1V reverse voltage range is the optimum voltage range for the operation of the photodiode with high responsivity.
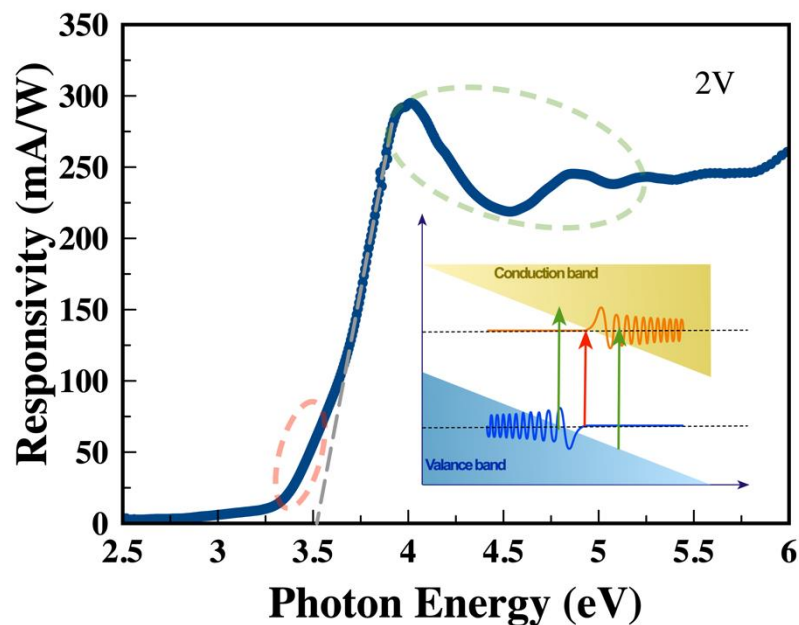


**Figure 5**. The spectral responsivity of homojunction p-type NiO:Mg/i-NiO / n-type NiO:Cu photodiode under -2V reverse bias and inserted schematic illustration of Franz-Keldysh effect.

Figure 5 shows the spectral responsivity of homojunction p-type NiO:Mg/i-NiO/n-type NiO:Cu photodiode under -2V reverse bias. It shows a spectral photoresponse characteristic of classic homojunction p-i-n photodiode with a peak responsivity of 295 mA/W of at 3.9 eV. The highest peak energy in spectral responsivity can be attributed to the bandgap energy of active material, which is NiO in this study [50]. Moreover, with three different slopes, an exponential-like increment has been observed from the lower photon energy to that of the higher and an oscillatory behaviour in responsivity of the photodiode is observed above the bandgap. These trends can be explained by the Franz–Keldysh effect.

Franz–Keldysh effect is a physical phenomenon associated with the influence of a high electric field on near-band-edge absorption [51,52]. It may cause a red shift of the absorption edge, giving rise to the presence of an absorption tail below the bandgap and an oscillatory behaviour in the frequency of the optical properties of the semiconductor is revealed above the energy of the bandgap (inserted in Figure 5) [53]. It is well-known phenomena in the literature on thin-film semiconductors and high-current photodetectors [51]. In other respects, the tail below the bandgap and nearly flat high responsivity above the bandgap compared to the NiO-based metal-semiconductor-metal photodetectors which show an interminable reduction of responsivity at the higher energy can also be attributed to the incorporation of the Cu and Mg atoms to the top and bottom NiO layers, respectively. The incorporation of Cu and Mg atoms with high concentration may forms alloying, which may cause blue and red-shift in the bandgap, respectively. Unveiling the dynamics of the doping mechanisms will be the future work.

## Conclusion

In this study, by introducing p-type NiO:Mg / i-NiO / n-type NiO:Cu homojunction p-i-n diode, we reported the growth, fabrication, and diode parameters as well as photodetector characteristics of a novel photodiode. The homojunction p-type NiO / i-NiO / n-type NiO has revealed good diode characteristics as well as rectification. These results show that Mg and Cu are promising doping atoms for NiO to have p-type and n-type doping characteristics, respectively. A nearly flat photoresponse on the p-i-n photodiode in between 3.75 eV and 6 eV with a responsivity of 250 mA/W was observed. Moreover, under forward bias, a negative capacitance effect which is attributed to radiative recombination in the active region is observed. These results may pave the way for fabricating highly sensitive photodetectors and efficient LEDs / lasers based on homojunction p-i-n NO for ultraviolet applications.

## Acknowledgements

## References

[1] A.B. Huang, J.T. Zhu, J.Y. Zheng, Y. Yu, Y. Liu, S.W. Yang, S.H. Bao, L. Lei, P. Jin, Achieving high-performance planar perovskite solar cells with co-sputtered Co-doping NiO x hole transport layers by efficient extraction and enhanced mobility, J Mater Chem C. 4 (2016) 10839–10846. https://doi.org/10.1039/c6tc03624d.

[2] S. Zhuang, J. He, X. Ma, Y. Zhao, H. Wang, B. Zhang, Fabrication and optimization of hole transport layer NiO for all inorganic perovskite light emitting diodes, Mat Sci Semicon Proc. 109 (2020) 104924. https://doi.org/10.1016/j.mssp.2020.104924.

[3] L. Zhao, X. Sun, Q. Yao, S. Huang, L. Zhu, J. Song, Y. Zhao, Y. Qiang, Field-Effect Control in Hole Transport Layer Composed of Li:NiO/NiO for Highly Efficient Inverted Planar Perovskite Solar Cells, Adv Mater Interfaces. 9 (2022) 2101562. https://doi.org/10.1002/admi.202101562.

[4] F. Sarcan, S. Orchard, B. Kuerbanjiang, A. Skeparovski, V.K. Lazarov, A. Erol, Ultraviolet Photodetector Based on Mg0.67Ni0.33O Thin Film on SrTiO3, Phys Status Solidi Rrl Rapid Res Lett. 14 (2020) 2000175. https://doi.org/10.1002/pssr.202000175.

[5] J.W. Mares, R.C. Boutwell, M. Wei, A. Scheurer, W.V. Schoenfeld, Deep-ultraviolet photodetectors from epitaxially grown NixMg1−xO, Appl Phys Lett. 97 (2010) 161113. https://doi.org/10.1063/1.3503634.

[6] H.-Y. Lee, C.-W. Lin, C.-T. Lee, Aluminum-nanosphere-stacked MgNiO metal-semiconductor-metal ultraviolet photodetectors, J Alloy Compd. 773 (2019) 210–216. https://doi.org/10.1016/j.jallcom.2018.09.256.

[7] Y. Zhao, J. Zhang, D. Jiang, C. Shan, Z. Zhang, B. Yao, D. Zhao, D. Shen, MgNiO-based metal–semiconductor– metal ultraviolet photodetector, J Phys D Appl Phys. 42 (2009) 092007. https://doi.org/10.1088/0022-3727/42/9/092007.

[8] A. Kerrigan, K. Pande, D. Pingstone, S.A. Cavill, M. Gajdardziska-Josifovska, K.P. McKenna, M. Weinert, V.K. Lazarov, Nano-faceted stabilization of polar-oxide thin films: The case of MgO(111) and NiO(111) surfaces, Appl Surf Sci. 596 (2022) 153490. https://doi.org/10.1016/j.apsusc.2022.153490.

[9] M. Budde, T. Remmele, C. Tschammer, J. Feldl, P. Franz, J. Lähnemann, Z. Cheng, M. Hanke, M. Ramsteiner, M. Albrecht, O. Bierwagen, Plasma-assisted molecular beam epitaxy of NiO on GaN(00.1), J Appl Phys. 127 (2020) 015306. https://doi.org/10.1063/1.5129881.

[10] S.D. Peacor, T. Hibma, Reflection high-energy electron diffraction study of the growth of NiO and CoO thin films by molecular beam epitaxy, Surf Sci. 301 (1994) 11–18. https://doi.org/10.1016/0039-6028(94)91283-1.

[11] P. Salunkhe, M.A. A.V, D. Kekuda, Structural, spectroscopic and electrical properties of dc magnetron sputtered NiO thin films and an insight into different defect states, Appl Phys. 127 (2021) 390. https://doi.org/10.1007/s00339-021-04501-0.

[12] M. Tachiki, T. Hosomi, T. Kobayashi, Room-Temperature Heteroepitaxial Growth of NiO Thin Films using Pulsed Laser Deposition, Jpn J Appl Phys. 39 (2014) 1817. https://doi.org/10.1143/jjap.39.1817.

[13] C.-W. Lin, W.-C. Chung, Z.-D. Zhang, M.-C. Hsu, P-channel transparent thin-film transistor using physical-vapor-deposited NiO layer, Jpn J Appl Phys. 57 (2017) 01AE01. https://doi.org/10.7567/jjap.57.01ae01.

[14] H.M. Yates, J.L. Hodgkinson, S.M.P. Meroni, D. Richards, T.M. Watson, Flame Assisted Chemical Vapour Deposition of NiO hole transport layers for planar perovskite cells, Surf Coatings Technology. 385 (2020) 125423. https://doi.org/10.1016/j.surfcoat.2020.125423.

[15] Z. Hu, D. Chen, P. Yang, L. Yang, L. Qin, Y. Huang, X. Zhao, Sol-gel-processed yttrium-doped NiO as hole transport layer in inverted perovskite solar cells for enhanced performance, Appl Surf Sci. 441 (2018) 258–264. https://doi.org/10.1016/j.apsusc.2018.01.236.

[16] R. Debnath, T. Xie, B. Wen, W. Li, J.Y. Ha, N.F. Sullivan, N.V. Nguyen, A. Motayed, A solution-processed high-efficiency p-NiO/n-ZnO heterojunction photodetector, Rsc Adv. 5 (2015) 14646–14652. https://doi.org/10.1039/c4ra14567d.

[17] M. Patel, J. Kim, Transparent NiO/ZnO heterojunction for ultra-performing zero-bias ultraviolet photodetector on plastic substrate, J Alloy Compd. 729 (2017) 796–801. https://doi.org/10.1016/j.jallcom.2017.09.158.

[18] S.-Y. Tsai, M.-H. Hon, Y.-M. Lu, Fabrication of transparent p-NiO/n-ZnO heterojunction devices for ultraviolet photodetectors, Solid State Electron. 63 (2011) 37–41. https://doi.org/10.1016/j.sse.2011.04.019.

[19] M. Patel, H. Kim, J. Kim, All Transparent Metal Oxide Ultraviolet Photodetector, Adv Electron Mater. 1 (2015) 1500232. https://doi.org/10.1002/aelm.201500232.

[20] M. Patel, H.-S. Kim, J. Kim, J.-H. Yun, S.J. Kim, E.H. Choi, H.-H. Park, Excitonic metal oxide heterojunction (NiO/ZnO) solar cells for all-transparent module integration, Sol Energ Mat Sol C. 170 (2017) 246–253. https://doi.org/10.1016/j.solmat.2017.06.006.

[21] T.T. Nguyen, M. Patel, S. Kim, R.A. Mir, J. Yi, V.-A. Dao, J. Kim, Transparent photovoltaic cells and self-powered photodetectors by TiO2/NiO heterojunction, J Power Sources. 481 (2021) 228865. https://doi.org/10.1016/j.jpowsour.2020.228865.

[22] P. Mahala, M. Patel, D.-K. Ban, T.T. Nguyen, J. Yi, J. Kim, High-performing self-driven ultraviolet photodetector by TiO2/Co3O4 photovoltaics, J Alloy Compd. 827 (2020) 154376. https://doi.org/10.1016/j.jallcom.2020.154376.

[23] Y. Wang, C. Wu, D. Guo, P. Li, S. Wang, A. Liu, C. Li, F. Wu, W. Tang, All-Oxide NiO/Ga2O3 p–n Junction for Self-Powered UV Photodetector, Acs Appl Electron Mater. 2 (2020) 2032–2038. https://doi.org/10.1021/acsaelm.0c00301.

[24] M.I. Pintor-Monroy, D. Barrera, B.L. Murillo-Borjas, F.J. Ochoa-Estrella, J.W.P. Hsu, M.A. Quevedo-Lopez, Tunable Electrical and Optical Properties of Nickel Oxide (NiO x ) Thin Films for Fully Transparent NiO x –Ga2O3 p–n Junction Diodes, Acs Appl Mater Inter. 10 (2018) 38159–38165. https://doi.org/10.1021/acsami.8b08095.

[25] J.D. Hwang, Y.T. Hwang, Enhancing ultraviolet-to-visible rejection ratio by inserting an intrinsic NiO layer in p-NiO/n-Si heterojunction photodiodes, Nanotechnology. 31 (2020) 345205. https://doi.org/10.1088/1361-6528/ab92ca.

[26] S. Chaoudhary, A. Dewasi, R.P. S, V. Rastogi, R.N. Pereira, A. Sinopoli, B. Aissa, A. Mitra, Laser ablation fabrication of a p-NiO/n-Si heterojunction for broadband and self-

powered UV-Visible-NIR photodetection, Nanotechnology. (2022).
https://doi.org/10.1088/1361-6528/ac5ca6.

[27] M. Budde, C. Tschammer, P. Franz, J. Feldl, M. Ramsteiner, R. Goldhahn, M. Feneberg, N. Barsan, A. Oprea, O. Bierwagen, Structural, optical, and electrical properties of unintentionally doped NiO layers grown on MgO by plasma-assisted molecular beam epitaxy, J Appl Phys. 123 (2018) 195301. https://doi.org/10.1063/1.5026738.

[28] S.C. Chen, T.Y. Kuo, S.U. Jen, H.P. Chiang, W.Y. Liu, C.H. Wang, Effect of copper content on the electrical stability of nickel oxide films, Thin Solid Films. 584 (2015) 238–242. https://doi.org/10.1016/j.tsf.2014.11.085.

[29] R. K, H. Reddy, U. S, Studies on the structural, electrical and optical properties of thermally oxidized copper nickel oxide thin films, Frontiers Nanosci Nanotechnol. 3 (2017). https://doi.org/10.15761/fnn.1000154.

[30] S.W. Fan, L. Yang, Y. Chen, B. Dou, The origin of the P-type conductivity for Cu and Ag-doped NiO: Density functional theory study, Mater Today Commun. 33 (n.d.) 104552. https://doi.org/10.1016/j.mtcomm.2022.104552.

[31] N.A. Kuruoğlu, O. Özdemir, K. Bozkurt, S. Belahsene, A. Martinez, A. Ramdane, Simultaneous Determination of Electron and Hole Mobilities in InP/InGaAsP/InAs/InP Laser Heterostructure by Admittance Spectroscopy, IEEE Transactions on Electron Devices. 64 (2017). https://doi.org/10.1109/TED.2017.2705719.

[32] E. Ehrenfreund, C. Lungenschmied, G. Dennler, H. Neugebauer, N.S. Sariciftci, Negative capacitance in organic semiconductor devices: Bipolar injection and charge recombination mechanism, Appl Phys Lett. 91 (2007) 012112. https://doi.org/10.1063/1.2752024.

[33] F. Lemmi, N.M. Johnson, Negative capacitance in forward biased hydrogenated amorphous silicon p+-i-n+ diodes, Appl Phys Lett. 74 (1999) 251–253. https://doi.org/10.1063/1.123271.

[34] K. Bansal, M. Henini, M.S. Alshammari, S. Datta, Dynamics of electronic transitions and frequency dependence of negative capacitance in semiconductor diodes under high forward bias, Appl Phys Lett. 105 (2014) 123503. https://doi.org/10.1063/1.4896541.

[35] D.-P. Han, Y.-J. Kim, J.-I. Shim, D.-S. Shin, Forward-Capacitance Measurement on Wide-Bandgap Light-Emitting Diodes, Ieee Photonic Tech L. 28 (2016) 2407–2410. https://doi.org/10.1109/lpt.2016.2597158.

[36] C.Y. Zhu, L.F. Feng, C.D. Wang, H.X. Cong, G.Y. Zhang, Z.J. Yang, Z.Z. Chen, Negative capacitance in light-emitting devices, Solid State Electron. 53 (2009) 324–328. https://doi.org/10.1016/j.sse.2009.01.002.

[37] D. Nag, T. Aggarwal, S. Sinha, R. Sarkar, S. Bhunia, Y.-F. Chen, S. Ganguly, D. Saha, R.-H. Horng, A. Laha, Carrier-Induced Defect Saturation in Green InGaN LEDs: A Potential Phenomenon to Enhance Efficiency at Higher Wavelength Regime, Acs Photonics. 8 (2021) 926–932. https://doi.org/10.1021/acsphotonics.0c01969.

[38] B. Saha, K. Sarkar, A. Bera, K. Deb, R. Thapa, Schottky diode behaviour with excellent photoresponse in NiO/FTO heterostructure, Appl Surf Sci. 418 (2017) 328–334. https://doi.org/10.1016/j.apsusc.2017.01.142.

[39] K. Ueno, K. Shibahara, A. Kobayashi, H. Fujioka, Vertical p-type GaN Schottky barrier diodes with nearly ideal thermionic emission characteristics, Appl Phys Lett. 118 (2021) 022102. https://doi.org/10.1063/5.0036093.

[40] S. Mahato, D. Biswas, L.G. Gerling, C. Voz, J. Puigdollers, Analysis of temperature dependent current-voltage and capacitance-voltage characteristics of an Au/V2O5/n-Si Schottky diode, Aip Adv. 7 (2017) 085313. https://doi.org/10.1063/1.4993553.

[41] H. Norde, A modified forward I - V plot for Schottky diodes with high series resistance, J Appl Phys. 50 (1979) 5052–5053. https://doi.org/10.1063/1.325607.

[42] S.K. Cheung, N.W. Cheung, Extraction of Schottky diode parameters from forward current-voltage characteristics, Appl Phys Lett. 49 (1986) 85–87. https://doi.org/10.1063/1.97359.

[43] N. Balkan, A. Erol, F. Sarcan, L.F.F. Al-Ghuraibawi, M.S. Nordin, Dilute nitride resonant cavity enhanced photodetector with internal gain for the $\lambda \sim 1.3\mu m$ optical communications window, Superlattice Microst. 86 (2015) 467–471. https://doi.org/10.1016/j.spmi.2015.07.032.

[44] F. Sarcan, Y. Wang, T.F. Krauss, T. Erucar, A. Erol, Dilute nitride resonant-cavity light emitting diode, Opt Laser Technology. 122 (2020) 105888. https://doi.org/10.1016/j.optlastec.2019.105888.

[45] B.J. Kim, J.H. Jeong, E.Y. Jung, T.Y. Kim, S. Park, J.-A. Hong, K.-M. Lee, W. Jeon, Y. Park, S.J. Kang, A visible-light phototransistor based on the heterostructure of ZnO and TiO2 with trap-assisted photocurrent generation†, Rsc Adv. 11 (2021) 12051–12057. https://doi.org/10.1039/d1ra00801c.

[46] N.A. Kuruoğlu, O. Özdemir, K. Bozkurt, S. Sundaram, J.-P. Salvestrini, A. Ougazzaden, Q. Gaimard, S. Belahsene, K. Merghem, A. Ramdane, Dc and ac electrical response of MOCVD grown GaN in p-i-n structure, assessed through I–V and admittance measurement, J Phys D Appl Phys. 50 (2017) 505109. https://doi.org/10.1088/1361-6463/aa98b2.

[47] M.A. Py, L. Lugani, Y. Taniyasu, J.-F. Carlin, N. Grandjean, Capacitance behavior of InAlN Schottky diodes in presence of large concentrations of shallow and deep states related to oxygen, J Appl Phys. 117 (2015) 185701. https://doi.org/10.1063/1.4919846.

[48] F. Kuruolu, M. alkan, S. Yldrm, M. Serin, Detailed study on effects of gate voltage, frequency and temperature on dielectric properties of Cu/PAr/n-CdS/SnO2 MIS Schottky diode, J Phys D Appl Phys. 54 (2021) 145102. https://doi.org/10.1088/1361-6463/abd80e.

[49] F. Kuruolu, M. alkan, M. Serin, A. Erol, Well-ordered nanoparticle arrays for floating gate memory applications, Nanotechnology. 31 (2020) 215203. https://doi.org/10.1088/1361-6528/ab7043.

[50] F. Sarcan, M. Aydin, F. Kuruoğlu, O. Donmez, S. Yildirim, A. Erol, Temperature-dependent sandwich and in-plane optical characterization of ternary chalcogenide TlSbS2, Mater Sci Eng B. 272 (2021) 115322. https://doi.org/10.1016/j.mseb.2021.115322.

[51] F. Sarcan, F. Nutku, M.S. Nordin, A.J. Vickers, A. Erol, A study on the voltage-dependent response of a GaInNAs-based pin photodetector with a quasi-cavity, Semicond Sci Tech. 33 (2018) 114006. https://doi.org/10.1088/1361-6641/aae074.

[52] M. Schmid, M. Kaschel, M. Gollhofer, M. Oehme, J. Werner, E. Kasper, J. Schulze, Franz–Keldysh effect of germanium-on-silicon p–i–n diodes within a wide temperature range, Thin Solid Films. 525 (2012) 110–114. https://doi.org/10.1016/j.tsf.2012.10.087.

[53] H. Taya, Franz-Keldysh effect in strong-field QED, Phys Rev D. 99 (2019) 056006. https://doi.org/10.1103/physrevd.99.056006.